Modelling and Optimization of Surface Roughness in Wood Powder/PLA Composites

Eleni Semertzidou[1], Athanasios Manavis[2], Nikolaos Efkolidis[1], Valerio Perna[3], Nikolla Vesho[4] and Panagiotis Kyratsis[1,*]

[1]*Department of Product and Systems Design Engineering, University of Western Macedonia, Kila, Kozani GR50100, Greece*

[2]*Department of Interior Architecture, International Hellenic University (IHU), Terma Magnisias, GR62124 Serres, Greece*

[3]*Department of Architecture, EPOKA University, Rruga Tiranë-Rinas, Km 12, 1039, Tirana/Albania*

[4]*Department of Architecture and Civil Engineering, Polis University, Rruga Bylis 12, SH2, 1051 Tirana, Albania*

Abstract: Fused filament fabrication (FFF) of wood-filled polylactic acid (Wood/PLA) offers an alternative for manufacturing components with a wood-like appearance. However, achieving consistent surface quality remains a challenge, particularly for components incorporating both internal and external surfaces. This study investigates the effects of flow rate, layer height, and printing speed on the surface roughness of FFF-manufactured Wood/PLA specimens. A three-factor, three-level full factorial experimental design comprising 27 parameter combinations was employed. Hollow cylindrical specimens were fabricated using a Bambu™ Lab A1 Mini printer, and internal and external surface roughness were measured using a stylus profilometer. Separate quadratic regression models were developed, and their statistical performance was evaluated using analysis of variance and regression diagnostics. The models exhibited coefficients of determination of 99.60% for internal roughness and 99.58% for external roughness. Layer height was the dominant factor associated with both responses, with increasing layer height from 0.20 to 0.40mm accompanied by substantial increases in measured roughness. Multi-response optimization identified a model-predicted candidate combination comprising a flow rate of 90.9%, a layer height of 0.20mm, and a printing speed of 116.0mm/s. The corresponding predicted roughness values were 13.648μm for the internal surface and 13.228μm for the external surface, with a composite desirability of approximately 0.998. Experimental confirmation was subsequently performed using three additional specimens corresponding to the multi-response and individual-response optimization solutions. The measured roughness values showed good agreement with the model predictions, with relative deviations below 3.2% across all comparisons. These findings highlight the dominant influence of layer height and support the applicability of the developed regression models for optimizing internal and external surface roughness within the investigated parameter range.

Keywords: Additive manufacturing, Fused filament fabrication, Process optimization, Response surface methodology, Surface roughness, Wood-PLA composite.

1. INTRODUCTION

Additive Manufacturing (AM), particularly Fused Filament Fabrication (FFF) or Fused Deposition Modelling (FDM), has revolutionized direct digital manufacturing across industrial, architectural, and consumer sectors [1, 2]. The increasing demand for sustainable materials has accelerated the adoption of bio-based thermoplastic composites, such as Polylactic Acid (PLA) filled with natural wood powder or wood fibres [3]. Wood-PLA bio-composites combine the biodegradability and dimensional stability of PLA with the tactile, aesthetic, and environmental advantages of natural wood [4]. Recent advancements have expanded their use from decorative items to functional furniture components [5] and complex structural assemblies [6]. However, the inclusion of wood fibres introduces rheological complexities; as noted by Bhayana *et al*. [7], the interaction between wood particles and the polymer matrix significantly affects the flow behaviour and, consequently, the final surface topography.

Despite their growing popularity, 3D printing of wood-filled polymers introduces distinct manufacturing complexities. Natural wood particles are inherently hygroscopic and thermally sensitive, which can lead to moisture-induced foaming, nozzle clogging, increased melt viscosity, and inter-layer voids [8, 9]. Furthermore, the layer-by-layer deposition intrinsic to FFF generates a characteristic 'stair-stepping' topography that significantly degrades surface finish [4, 9, 10]. In functional engineering components—particularly those featuring internal bores, cylindrical assemblies, or fluid conduits—surface roughness (Ra) directly impacts friction, dimensional tolerance, wear resistance, and fatigue life [11, 12].

Previous studies have investigated the influence of primary printing parameters on the mechanical

*Address correspondence to this author at the Department of Product and Systems Design Engineering, University of Western Macedonia, Kila, Kozani GR50100, Greece;
E-mail: pkyratsis@uowm.gr

Received on 11-09-2026 Accepted on 26-10-2026 Published on 03-11-2026

E-ISSN: 2311-8717/26

properties and surface quality of PLA and composite filaments [12]. In particulate-filled and functional composite filaments, full factorial designs and Response Surface Methodology (RSM) have proven highly effective in quantifying how process parameters—such as material flow rate, layer thickness, and temperature—govern material deposition, layer bonding, and final performance [13, 14]. Research on wood-filled composites has shown that layer height and extrusion temperature strongly affect tensile strength and surface finish [6, 15, 16]. However, a critical research gap remains: most existing literature evaluates surface roughness solely on flat test bars or exterior convex surfaces, neglecting the comparative roughness behaviour between internal concave features (bores/holes) and external convex surfaces under identical printing conditions. Internal and external surfaces may exhibit different roughness characteristics because of differences in toolpath geometry, material deposition patterns, and local printing conditions [10]. However, comparative experimental investigations of internal and external surface roughness under identical processing conditions remain valuable for understanding these differences in FFF-manufactured components.

To address this gap, the objective of the present study is to systematically model, compare, and optimize the surface roughness of Wood Powder/PLA composites across internal bore (Ra IN) and external cylindrical (Ra OUT) surfaces. Utilizing a 3^3 Full Factorial Response Surface Methodology (RSM) with 27 experimental runs, this work investigates the combined effects of flow rate, layer height, and printing speed. Quadratic regression models and Analysis of Variance (ANOVA) are employed to quantify main and interaction effects, followed by Desirability Function multi-response optimization.

2. MATERIALS AND METHODS

2.1. Material Characterization and Preparation

The specimens were fabricated using a commercial wood-filled polylactic acid (Wood/PLA) filament, specifically BambuTM Lab PLA Wood in "Clay Brown" (Product Code: 13801). As stated in the manufacturer's Safety Data Sheet (MSDS) [17], the material contains 70–85 wt% polylactic acid (PLA), 10–18 wt% wood powder, and 5–12 wt% additives. The filament has a nominal diameter of 1.75 ± 0.03 mm and a reported density of 1.21 g/cm³ according to the manufacturer's Technical Data Sheet (TDS) [18]. Additional manufacturer-reported properties include a melt flow index of 29.4 ± 1.7 g/10 min (210°C, 2.16 kg), a glass transition temperature of 54°C, and a melting temperature of 156°C [18]. These composition ranges are manufacturer-reported values and were not independently verified for the specific filament batch used in this study.

Given the hygroscopic nature of natural wood particulates, which can lead to moisture-induced foaming and degradation of surface finish, a drying protocol was implemented. The filament was pre-dried in a Creality™ Filament Dry Box 2.0 at 55°C for 8 hours. To ensure process consistency and prevent re-absorption of ambient moisture, the filament was maintained at a constant temperature of 45°C within the dry box throughout the entire printing duration.

2.2. 3D Printing Hardware and Process Parameters

Fabrication was performed on a Bambu™ Lab A1 Mini FFF system. A 0.6 mm hardened steel nozzle was selected to mitigate nozzle clogging due to fibre bridging, a common failure mode in particulate-filled

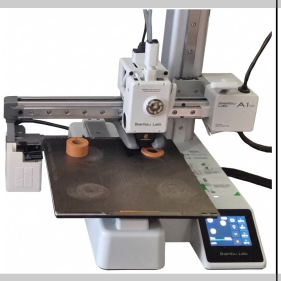
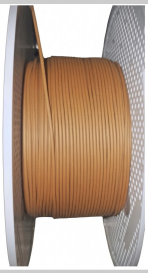
3D Printer	Filament	Filament Dryer	Roughness Instrument
			
Bambu Lab A1 Mini	**Bambu Lab PLA Wood** (13801)	**Creality Filament Dry Box 2.0**	**Diavite DH-8**
• FDM/FFF 3D Printer • Build Volume: 180*180*180mm • 0.6mm Hardened Steel Nozzle • Textured PEI Build Plate	• Wood powder content: 10–18 wt% • 1.75 mm diameter • Density: 1.21 g/cm3 • Recommended Nozzle & Bed temperature (with glue): 190-240˚C & 35 – 45°C	• Temperature Range: 45-65°C • 360° Hot-air heating • Filament Drying at 55°C for 8h • Filament Maintained at 45 °C during printing	• Stylus profilometer • Display Ra: 0.001µm • Tracing skid radius: 25 mm (standard tracer) • Tracing length: 5mm • Tracing Speed: 0.5 mm/s • Reverse speed: 1.0 mm/s

Figure 1: The experimental setup /equipment of the research.

Table 1: The Three Variable Parameters and their Three Levels

Factor	Symbol	Level -1	Level 0	Level +1
Flow Rate (%)	**Flow**	80	95	110
Layer Height (mm)	**Layer**	0.20	0.30	0.40
Printing Speed (mm/s)	**Speed**	40	80	120

filaments [19]. While larger nozzles can inherently increase surface roughness, they are essential for process reliability in bio-composites [8]. The specimens were printed on a textured PEI (Polyetherimide) build plate to ensure robust first-layer adhesion.

The complete hardware configuration, including the specifications of the filament, the drying system, and the roughness measurement instrument (Diavite^{TM} DH-8), is illustrated in Figure **1**.

A full factorial experimental design with three factors, each investigated at three levels, was employed. The factors were flow rate, layer height, and printing speed. Their respective levels are presented in Table **1**. The design comprised (3^3=27) unique parameter combinations, and one specimen was printed individually for each combination.

The flow setting represents the extrusion percentage relative to the nominal material flow specified in the slicing software. Layer refers to the thickness of each deposited layer. Speed represents the selected speed profile applied to the printing operations, including the outer walls, inner walls, infill, and solid regions.

To isolate the effects of these variables, all other printing settings were kept constant, as detailed in Table **2**.

2.3. Specimen Design and Roughness Measurement

A hollow cylindrical specimen was designed using a general purposes computer-aided design (CAD) software. The specimen geometry incorporated a central through-hole to enable roughness measurements on both the external diameter and the internal bore diameter of the same specimen. The nominal external diameter was 30 mm, the internal diameter was 15 mm, and the specimen height was 15 mm (Figure **2a**).

The specimens were numbered from 1 to 27 to maintain traceability between the selected printing conditions and the subsequent roughness measurements. One physical specimen was fabricated for each of the 27 unique parameter combinations; therefore, the experimental design did not include independent replicate specimens at identical printing settings.

Table 2: Fixed 3D Printing Parameters used for All Specimens

Printing Parameter	Value	Printing Parameter	Value
Infill Density	50%	Wall loops	2
Nozzle Temperature	220ºC	Sparse Infill Pattern	Grid
Bed Temperature (with glue)	65ºC	Internal Solid Infill Pattern	Rectilinear
Cooling Fan	60-80%	Build Orientation	Horizontal

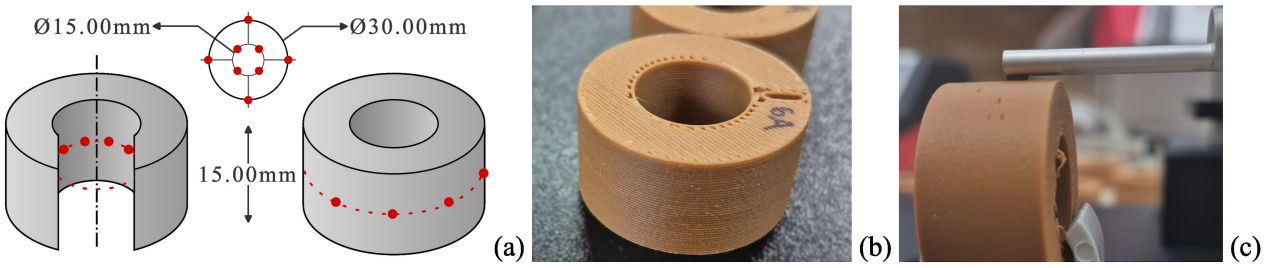


Figure 2: (**a**) Specimen geometry and surface roughness measurement locations. (**b**) A single cylindrical specimen. (**c**) Surface roughness testing.

Surface roughness was measured using a Diavite™ DH-8 stylus profilometer. The measurements were conducted perpendicular to the deposited layer lines to capture the peak-to-valley profile characteristic of the 'stair-stepping' effect (Figure **2b**). Four measurement locations distributed symmetrically around the circumference were selected on the external surface. Four corresponding locations were measured on the internal surface of the central hole (Figure **2c**). Thus, eight roughness readings were obtained from each specimen: four external readings and four internal readings.

The arithmetic mean roughness, (Ra), was used as the response variable. For each specimen, the four measurements obtained from the external surface and the four measurements obtained from the internal surface were averaged separately. Accordingly, the representative roughness values for each specimen were calculated as:

$$Ra\ IN=(Ra\ IN_1+ Ra\ IN_2+ Ra\ IN_3+ Ra\ IN_4)/4 \quad (1)$$

$$Ra\ OUT=(Ra\ OUT_1+ Ra\ OUT_2+ Ra\ OUT_3+ Ra\ OUT_4)/4 \quad (2)$$

where $Ra\ IN_i$ and $Ra\ OUT_i$ represent the individual roughness measurements at the four selected locations on the internal and external surfaces, respectively. The resulting average values were used as the response variables in the subsequent statistical analysis. Thus, each experimental run contributed one average internal roughness value and one average external roughness value.

The absence of independent replicate prints at identical parameter settings represents a methodological limitation of the experimental design. Consequently, the residual error of the regression models cannot be interpreted as a pure estimate of experimental error, as it may also include contributions from model lack-of-fit and other unexplained sources of variability. Furthermore, the specimen-to-specimen variability associated with repeated printing under identical conditions could not be independently quantified.

3. RESULTS AND DISCUSSION

3.1. Experimental Surface Roughness Trends

The results of the 27 experimental runs, as detailed in Table **3** indicate a clear distinction between internal and external surface roughness responses. Across the investigated conditions, layer height showed the clearest association with average roughness: increasing the layer height from 0.20 to 0.40mm was accompanied by a substantial increase in both internal and external Ra.

For the internal surface, the measured specimen average roughness ranged from 13.650 to 29.716 μm. The minimum recorded value occurred at a flow rate of 80%, a layer height of 0.20 mm, and a printing speed of 40mm/s. The maximum value was recorded at 80% flow, 0.40mm layer height, and 40mm/s.

For the external surface, the corresponding measured averages ranged from 13.163 to 26.875 μm. The minimum occurred at 80% flow, 0.20 mm layer

Table 3: The Averaged Measured Roughness Values of the Experiment

Run	Flow (%)	Layer (mm)	Speed (mm/s)	Ra IN (μm)	Ra OUT (μm)	Run	Flow (%)	Layer (mm)	Speed (mm/s)	Ra IN (μm)	Ra OUT (μm)
1	80	0.2	40	**13.650**	14.091	**15**	95	0.4	80	27.185	25.645
2	80	0.3	40	20.751	19.870	**16**	95	0.2	120	13.741	13.233
3	80	0.4	40	**29.716**	26.659	**17**	95	0.3	120	19.804	18.453
4	80	0.2	80	13.864	**13.163**	**18**	95	0.4	120	26.433	25.299
5	80	0.3	80	21.087	18.932	**19**	110	0.2	40	14.583	14.242
6	80	0.4	80	27.773	**26.875**	**20**	110	0.3	40	20.888	20.645
7	80	0.2	120	13.944	13.615	**21**	110	0.4	40	26.725	26.272
8	80	0.3	120	21.137	19.288	**22**	110	0.2	80	13.907	13.708
9	80	0.4	120	29.223	26.137	**23**	110	0.3	80	20.383	20.015
10	95	0.2	40	14.397	13.848	**24**	110	0.4	80	26.022	24.890
11	95	0.3	40	20.647	20.142	**25**	110	0.2	120	14.158	13.219
12	95	0.4	40	27.422	26.824	**26**	110	0.3	120	20.430	19.143
13	95	0.2	80	13.837	13.602	**27**	110	0.4	120	26.507	24.595
14	95	0.3	80	20.120	19.840						

height, and 80 mm/s, whereas the maximum occurred at 80% flow, 0.40 mm layer height, and 80 mm/s.

These ranges show that the lowest measured roughness values for both surfaces were obtained at the minimum tested layer height. However, the parameter combinations producing the lowest measured values were not identical for the two surfaces. This initial observation supports the necessity of separate modelling for internal and external topographies.

3.2. Statistical Analysis and Regression Modelling

The main effects plot (Figure **3a**) identifies layer height as the most critical parameter for both responses. Increasing the layer height from 0.20 to 0.40mm resulted in a pronounced increase in average roughness. In comparison, the effect of extrusion flow rate was smaller, with roughness decreasing from 80% to 95% flow and remaining approximately stable at 110%. Printing speed showed diverging effects: for the internal surface, a slight increase in roughness was noted at 120mm/s, whereas for the external surface, the response remained relatively stable and showed a minor decrease at higher speeds.

The comparison plot in Figure **3b**, further illustrates that the experimental results are clustered into three distinct regions based on layer height. A comparison of the internal and external surface roughness values revealed that the internal surface exhibited higher Ra values in 26 out of the 27 experimental runs. The only exception was Run 1, for which the internal and external roughness values were 13.650 µm and 14.091 µm, respectively. The internal surface exhibited a wider range of roughness values (13.650–29.716 µm) compared with the external surface (13.163–26.875 µm), indicating greater variation across the investigated printing conditions. The largest differences between the two surfaces were observed in Runs 3 and 9, amounting to 3.057 µm and 3.086 µm, respectively. Both runs were performed at a flow rate of 80% and a layer height of 0.4 mm, but at different printing speeds (40 and 120 mm/s). Conversely, the smallest differences were recorded in Runs 13 and 22, at 0.235 µm and 0.199 µm, respectively. These observations highlight that the difference between internal and external surface roughness was not constant across the experimental conditions.

To quantify these relationships, full second-order polynomial quadratic regression models were developed (Equations 3 and 4):

$$Ra\ IN = 20.087 - 0.419\ Flow + 6.718\ Layer - 0.189\ Speed + 0.421\ Flow^2 + 0.144\ Layer^2 + 0.322\ Speed^2 - 0.721\ Flow*Layer - 0.107\ Flow*Speed - 0.076\ Layer*Speed \quad (3)$$

$$Ra\ OUT = 19.450 - 0.1056\ Flow + 6.1374\ Layer - 0.5338\ Speed + 0.088\ Flow^2 + 0.181\ Layer^2 + 0.124\ Speed^2 - 0.351\ Flow*Layer - 0.218\ Flow*Speed - 0.134\ Layer*Speed \quad (4)$$

Statistical significance and factor contribution percentages were derived via Analysis of Variance (ANOVA), as summarized in Tables **4** and **5**. The process parameters were coded at three levels (−1, 0, and +1), corresponding to their respective low, central, and high experimental values. The quadratic models exhibited an excellent fit to the experimental data, with R^2 values exceeding 99.5% for both responses. The adjusted and predicted R^2 values were also high,

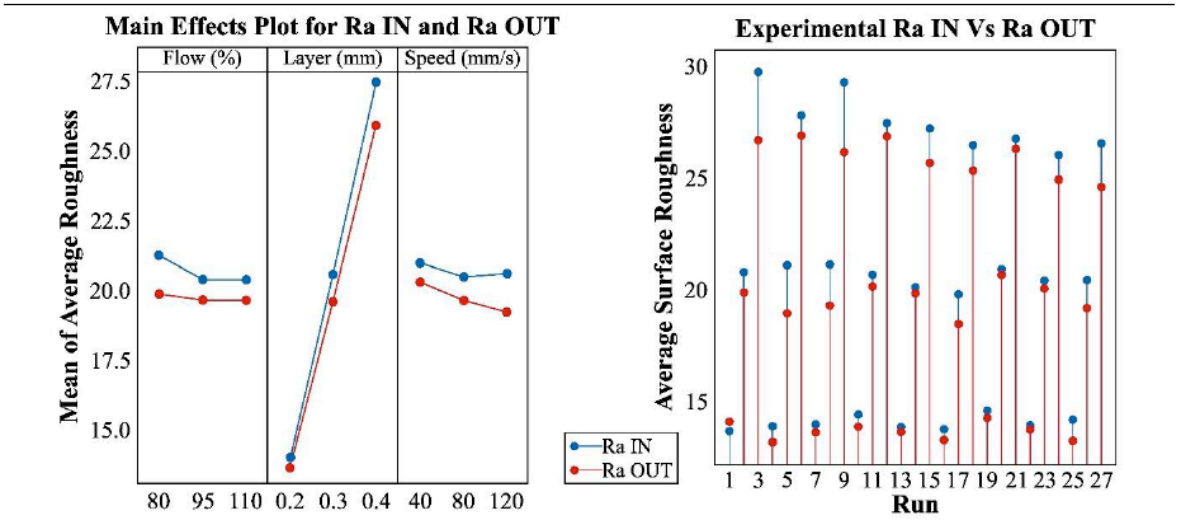


Figure 3: (**a**) Main effects plot for interior and exterior roughness. (**b**) Comparison between interior and exterior experimental roughness.

Table 4: Analysis of Variance for Exterior Roughness - Ra OUT

Source	Degree Of Freedom	Sum Of Squares	Mean Square	F-Value	P-Value	Contribution
Regression	9	685.948	76.216	442.90	0.000	99.58%
Error	17	2.925	0.172			0.42%
Total	26	688.874				100.00%
R-Sq: 99.58%		**R-Sq (Adj): 99.35%**		**R-Sq (Pred): 98.97%**		
Flow	1	0.201	0.201	1.17	0.295	0.03%
Layer	1	678.013	678.013	3939.97	0.000	98.42%
Speed	1	5.130	5.130	29.81	0.000	0.74%
Flow^2	1	0.047	0.047	0.27	0.609	0.01%
Layer^2	1	0.197	0.197	1.15	0.299	0.03%
Speed^2	1	0.093	0.093	0.54	0.473	0.01%
Flow*Layer	1	1.480	1.480	8.60	0.009	0.21%
Flow*Speed	1	0.572	0.572	3.33	0.086	0.08%
Layer*Speed	1	0.216	0.216	1.25	0.278	0.03%

Table 5: Analysis of Variance for Interior Roughness - Ra IN

Source	Degree Of Freedom	Sum Of Squares	Mean Square	F-Value	P-Value	Contribution
Regression	9	824.447	91.605	464.87	0.000	99.60%
Error	17	3.350	0.197			0.40%
Total	26	827.797				100.00%
R-Sq: 99.60%		**R-Sq (Adj): 99.38%**		**R-Sq (Pred): 98.84%**		
Flow	1	3.159	3.159	16.03	0.001	0.38%
Layer	1	812.394	812.394	4122.67	0.000	98.14%
Speed	1	0.643	0.643	3.26	0.089	0.08%
Flow^2	1	1.063	1.063	5.39	0.033	0.13%
Layer^2	1	0.125	0.125	0.63	0.438	0.02%
Speed^2	1	0.623	0.623	3.16	0.093	0.08%
Flow*Layer	1	6.233	6.233	31.63	0.000	0.75%
Flow*Speed	1	0.138	0.138	0.70	0.414	0.02%
Layer*Speed	1	0.070	0.070	0.35	0.560	0.01%

indicating good model performance within the investigated experimental domain.

For external roughness, layer height was by far the dominant parameter. Its linear term accounted for 98.42% of the total sum of squares, while printing speed accounted for a further 0.74%. Both parameters had statistically significant linear effects (p=0.000). The Flow*Layer interaction was also statistically significant (p=0.009), although its contribution to the total sum of squares was relatively small (0.21%). The remaining terms, including the linear effect of flow rate and all quadratic terms, were not statistically significant. The pronounced influence of layer height is also reflected in the experimental results, where increasing it from 0.2 mm to 0.4 mm resulted in an increase in average roughness from approximately 14.0 µm to 27.5 µm. This trend is consistent with the geometric stair-stepping effect associated with layer-by-layer material deposition.

A similar dominance of layer height was observed for internal roughness, with its linear term accounting for 98.14% of the total sum of squares. In contrast to the external surface, the linear effect of flow rate was also statistically significant (p = 0.001), although its contribution was comparatively small (0.38%). The quadratic term of flow rate was statistically significant as well (p = 0.033), suggesting a nonlinear relationship

between flow rate and internal surface roughness. Furthermore, the Flow*Layer interaction showed a statistically significant effect (p=0.000), accounting for 0.75% of the total sum of squares. This indicates that the effect of flow rate on internal roughness depends partly on the selected layer height. The linear effect of printing speed and the remaining quadratic and interaction terms were not statistically significant.

Overall, the ANOVA results confirm that layer height was the predominant parameter affecting both internal and external surface roughness. However, differences in the statistical significance of the other model terms indicate that the two surfaces respond somewhat differently to changes in the printing parameters.

It should be noted that the experimental design included one physical specimen per parameter combination, without independent replicate prints. Therefore, the residual error used in the regression analysis does not represent a pure estimate of experimental error, since it may also contain contributions from model lack-of-fit and other unexplained variability. As a result, the ANOVA results and associated significance tests should be interpreted with this limitation in mind. In particular, the experimental design does not allow an independent assessment of specimen-to-specimen variability or printing repeatability under identical conditions. The four roughness measurements obtained from each specimen were used to calculate a representative average response and should not be considered independent experimental replicates.

3.3. Predictive Accuracy and Response Surface Analysis

The residual diagnostic plots for the Ra OUT, suggest that the residuals are approximately centred around zero and broadly follow a near-normal pattern. The normal probability plot (Figure **4a**) shows most observations reasonably close to the reference line, and the histogram (Figure **4c**) is concentrated around zero. The residuals-versus-fitted-values plot (Figure **4b**) does not show a strong systematic change in spread, although some local variation is present. The residuals-versus-observation-order plot (Figure **4d**) shows fluctuations across the sequence of observations, which cannot be interpreted as evidence of independent repeatability because each experimental condition was represented by only one printed specimen. Overall, the plots do not indicate an obvious severe violation of the model assumptions, but they should be interpreted with the limitation that the design did not include replicate prints at identical settings.

The predictive capability of the models is further demonstrated in Figure **5**, where the relative error between experimental and predicted values remains below 4% across all 27 runs.

Figure **6** presents the contour plots of external (Ra OUT) and internal (Ra IN) surface roughness as functions of the investigated printing parameters. The layer height*flow rate plots (Figure **6a**, **d**) exhibit a clear variation in the predicted responses across the layer height range, while the contour patterns remain comparatively uniform along the flow rate direction.

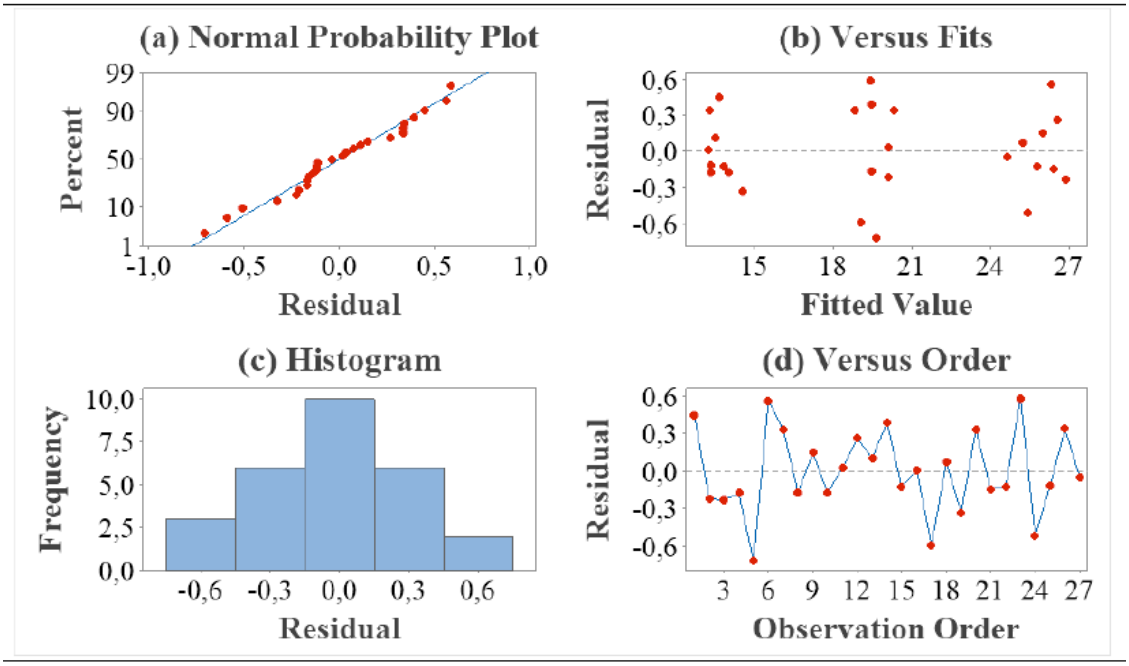


Figure 4: Residual plots for average outer roughness.

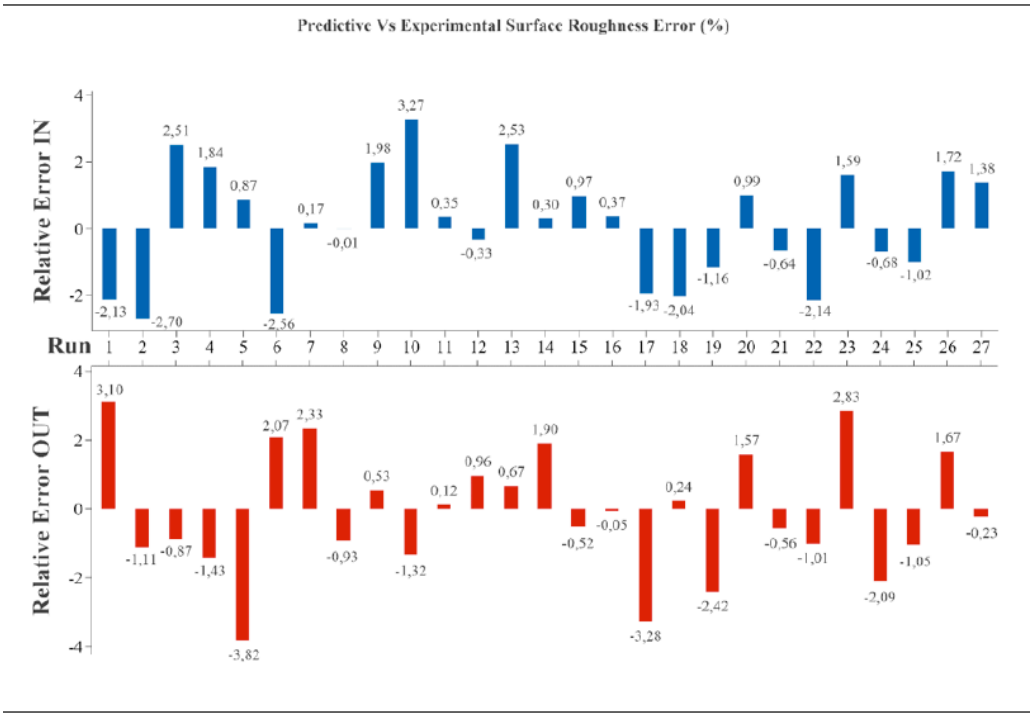


Figure 5: Comparison between predicted and experimental values.

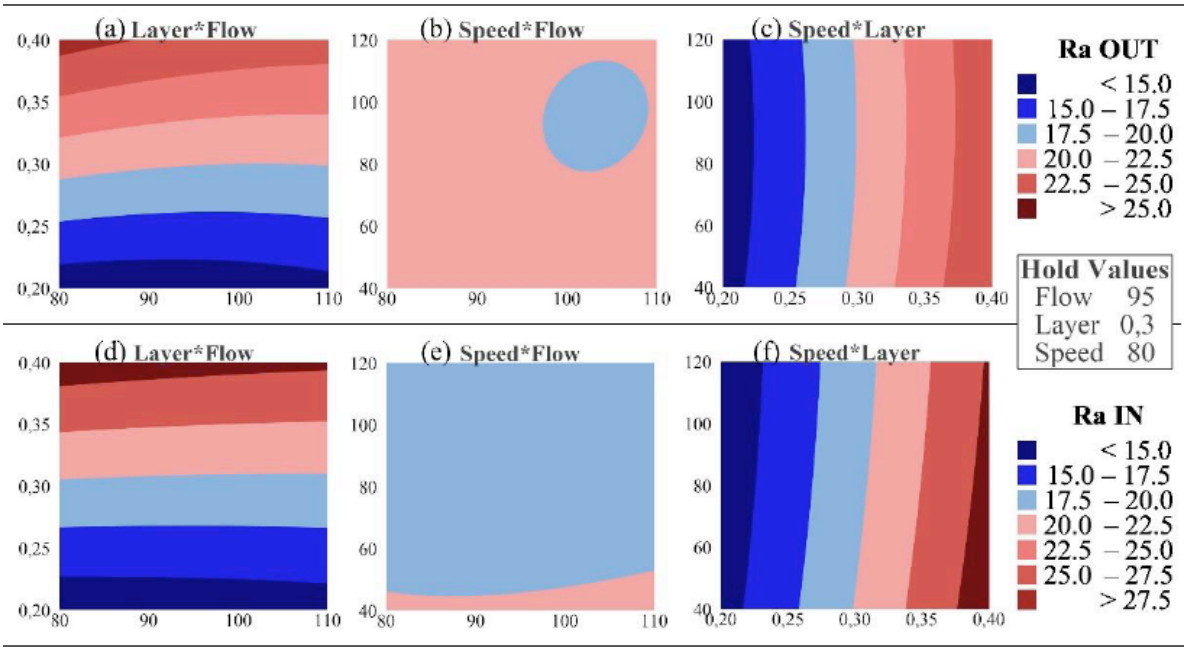


Figure 6: Contour plots of average inner and outer roughness.

Similarly, the layer height*speed plots (Figure **6c**, **f**) display distinct contour transitions with layer height, whereas the variation associated with printing speed is less pronounced. In contrast, the flow rate*speed plots (Figure **6b**, **e**), generated at the selected reference layer height, exhibit relatively uniform response regions, with localized contour variations indicating a more limited change in predicted roughness across the corresponding parameter ranges. Overall, the contour plots provide a visual representation of the response behaviour captured by the fitted quadratic models and complement the statistical findings reported in the preceding ANOVA analysis.

The three-dimensional response surface plots in Figure **7** illustrate the variation in predicted external and internal surface roughness across the investigated parameter combinations. The surfaces defined by layer height and flow rate (Figure **7a**, **b**, **d**, **e**) exhibit a pronounced slope along the layer height direction, while their profiles along the flow-rate axis are comparatively less steep. The flow rate–speed

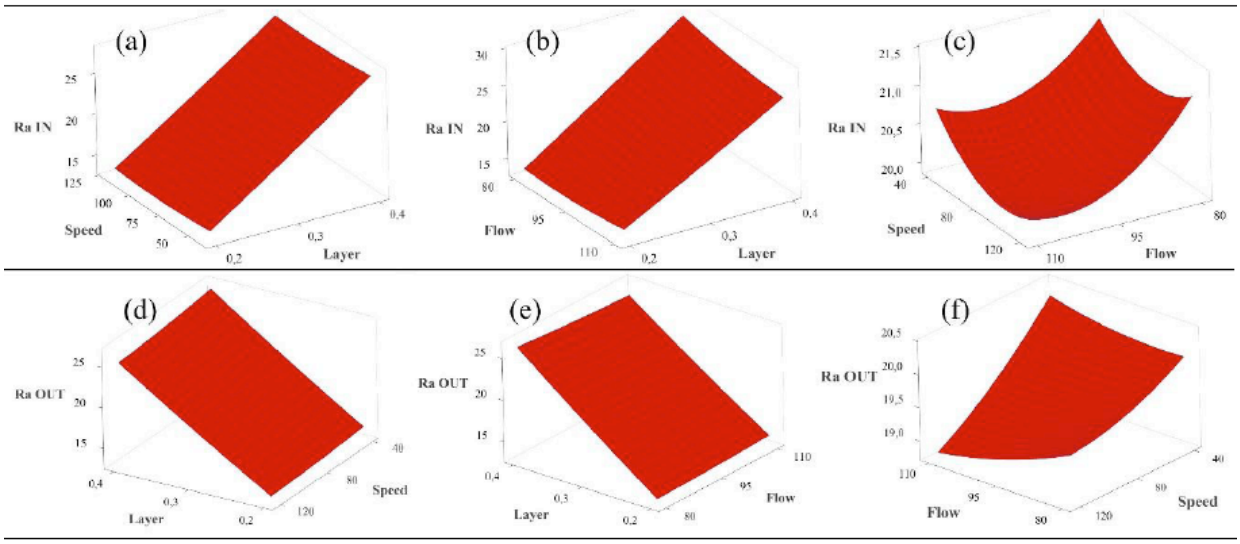


Figure 7: Surface plots of average inner and outer roughness.

surfaces (Figure **7c**, **f**) display a different response profile, characterized by a curved surface rather than a uniformly inclined plane, indicating a nonlinear variation in the predicted responses across these parameter combinations. These plots complement the contour analysis by providing a three-dimensional representation of the fitted models and illustrating the response profiles within the investigated experimental domain.

3.4. Physical Interpretation of Surface Roughness Behaviour

To contextualize the statistical regression models and response surface analysis, the observed roughness trends are discussed in relation to established FFF mechanisms reported in the literature. The following interpretations provide possible explanations for the observed behaviour; however, the corresponding physical mechanisms were not directly measured in the present study.

3.4.1. Layer Height Dominance and Geometric Stair-Stepping

ANOVA results identified layer height as the dominant process parameter for both internal and external surface roughness, accounting for 98.14% and 98.42% of the total sum of squares associated with the respective linear terms. This pronounced influence is consistent with the geometric 'stair-stepping' effect inherent to the layer-by-layer material deposition process [20]. Increasing the layer height from 0.20 mm to 0.40 mm produces coarser layer steps which may contribute to the higher measured arithmetic mean roughness (Ra). Conversely, smaller layer heights produce finer layer transitions and may result in smoother surface profiles. In wood-filled composites, the presence of dispersed wood particles may also influence the resulting surface topography; nevertheless, their individual contribution was not separately investigated in this study. In natural fibre biocomposites, smaller layer heights refine this geometry and promote a smoother envelope over embedded particles [21].

3.4.2. Non-Linear Flow Rate Influence and Parameter Interactions

The statistical analysis revealed differences in the influence of flow rate between the two surface geometries. For the internal surface, both the linear flow-rate term ($p = 0.001$) and its quadratic term ($p = 0.033$) were statistically significant, indicating a non-linear response within the investigated parameter range. In contrast, neither term was statistically significant for the external surface. The interaction between flow rate and layer height was significant for both internal ($p < 0.001$) and external ($p = 0.009$) roughness, suggesting that the effect of flow rate depends partly on the selected layer height.

These differences may be related to the distinct deposition conditions associated with concave and convex toolpaths. For example, variations in local material deposition, bead geometry, and thermal conditions could potentially influence the formation of the internal and external surface profiles differently. Previous research has also discussed the influence of wood-composite rheology and thermal behaviour on material deposition and dimensional changes [16]. However, since local pressure, temperature, and bead deformation were not measured in the present study, these explanations should be considered as possible interpretations rather than experimentally established mechanisms.

3.4.3. Influence of Printing Speed

The influence of printing speed also differed between the two surface responses. The linear speed term was statistically significant for external roughness ($p < 0.001$), whereas no statistically significant main effect was identified for internal roughness ($p = 0.089$). This indicates that the external surface response was more sensitive to changes in printing speed within the investigated range, although the effect should be interpreted in conjunction with the other process parameters.

Printing speed may influence the time available for material deposition, as well as the interaction between successive deposited beads. In addition, machine motion and process-control characteristics may affect the resulting deposition behaviour. Nevertheless, the present experimental design did not include direct measurements of these phenomena; therefore, their contribution to the observed surface roughness cannot be established independently.

3.4.4. Comparative Analysis of Internal Ra IN and External Ra OUT Surface Geometries

The comparison of internal and external surface roughness demonstrated that the two geometries did not respond identically to the investigated printing conditions. As discussed in Section 3.2, the internal surface generally exhibited higher roughness values, although this trend was not universal across all experimental runs. Furthermore, the individual-response optimization yielded different candidate parameter combinations for minimizing internal and external roughness, providing additional evidence of their distinct response behaviour.

The observed differences may be associated with the geometric characteristics of internal concave bores and external convex perimeters. Differences in toolpath configuration, local material deposition patterns, and thermal conditions could potentially affect bead formation and the resulting surface topography. For instance, the constrained geometry of an internal bore may lead to deposition conditions that differ from those encountered along an external perimeter. However, these explanations remain hypotheses, as the relevant local thermal and deposition phenomena were not directly monitored during printing.

Overall, the findings indicate that internal and external surface roughness should be considered separately when evaluating the surface quality of hollow Wood/PLA components. Their distinct statistical responses suggest that process conditions selected to improve one surface may not necessarily produce an equivalent improvement on the other.

3.5. Optimization and Experimental Confirmation

To identify the processing conditions that minimize surface roughness for both internal and external geometries, a numerical multi-response optimization was conducted using the Desirability Function Analysis (DFA). Both responses, internal surface roughness (Ra IN) and external surface roughness (Ra OUT), were assigned a minimization goal. The objective was to identify a combination of flow rate, layer height, and printing speed that minimizes both responses simultaneously by maximizing the composite desirability (D).

The Response Optimizer provided three alternative solutions for the combined optimization, alongside three solutions for each individual response, as summarized in Table **6**. For the multi-response optimization, Solution 1 yielded a model-predicted flow rate of 90.9%, a layer height of 0.20 mm, and a printing speed of 116.0 mm/s. The corresponding predicted roughness values were Ra IN=13.648 μm and Ra

Table 6: Optimization Solutions for Individual and Multiple Responses

Optimization Goal	Target	Upper	Solution	Flow (%)	Layer (mm)	Speed (mm/s)	Predicted Ra OUT (μm)	Predicted Ra IN (μm)	Composite Desirability (D)
Ra OUT & Ra IN	13.163 & 13.650	26.875 & 29.716	1	90.9	0.2	116.0	**13.228**	**13.648**	0.998
			2	80.0	0.2	40.0	13.642	13.960	0.973
			3	110.0	0.2	120.0	13.334	14.338	0.972
Ra OUT	13.163	26.875	1	92.7	0.2	120.0	**13.216**	-	0.996
			2	104.6	0.2	120.0	13.272	-	0.992
			3	80.0	0.2	120.0	13.280	-	0.992
Ra IN	13.650	29.716	1	89.7	0.2	84.4	-	**13.455**	1.000
			2	80.0	0.2	43.9	-	13.900	0.984
			3	80.0	0.2	120.0	-	14.206	0.965

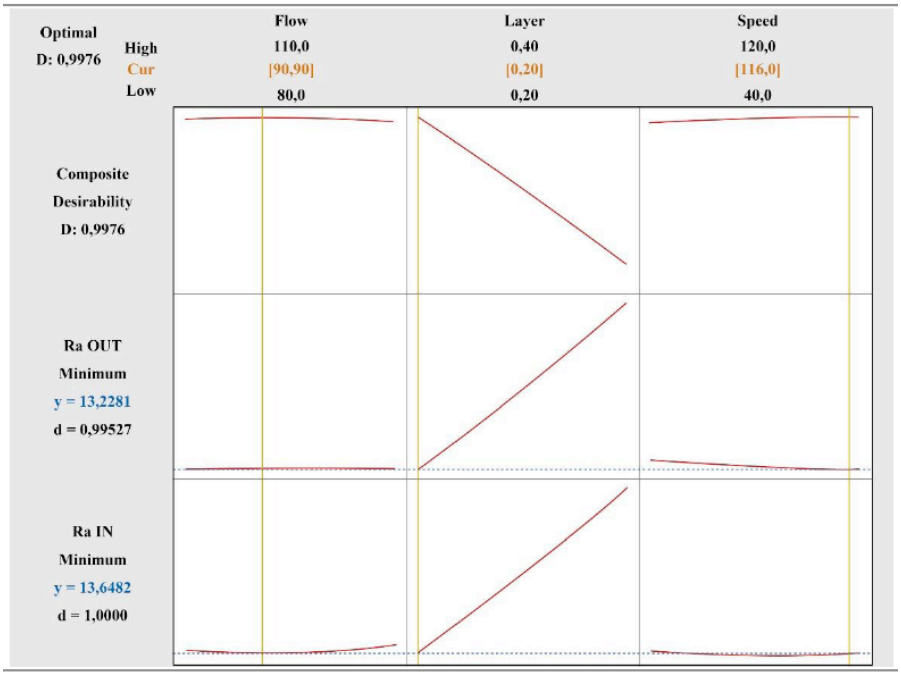


Figure 8: Multi-response optimization plot for internal and external surface roughness.

OUT=13.228 μm, with a composite desirability of D=0.998. This high desirability value indicates that the predicted responses closely satisfy the specified minimization objectives simultaneously.

All three multi-response solutions selected the minimum tested layer height of 0.20mm, further supporting the dominant influence of this parameter on surface roughness identified through regression modelling and ANOVA. Although the solutions differed in flow rate and printing speed, all exhibited high composite desirability values (D≥0.972) indicating that several alternative parameter combinations were predicted to provide similarly favourable surface finishes.

The individual-response optimization results further illustrate the differences between the two surface geometries. The minimum predicted internal roughness was obtained at a flow rate of 89.7%, a layer height of 0.20 mm, and a printing speed of 84.4mm/s, whereas the minimum predicted external roughness was obtained at a flow rate of 92.7%, a layer height of 0.20mm, and a printing speed of 120.0 mm/s. These differences demonstrate that optimizing the two responses separately does not necessarily lead to the same processing conditions. Consequently, multi-response optimization provides a useful approach for identifying a compromise solution when both internal and external surface quality are considered simultaneously.

To experimentally assess the optimization results, three confirmation specimens were manufactured, one for each set of optimized processing conditions. The first specimen corresponded to the multi-response solution, using a flow rate of 90.9%, a layer height of 0.20 mm, and a printing speed of 116.0 mm/s. The other two specimens were manufactured using the individual-response optimized settings for Ra OUT (92.7%, 0.20 mm, and 120.0 mm/s) and Ra IN (89.7%, 0.20 mm, and 84.4 mm/s), respectively. Surface roughness was measured following the same procedure as in the initial experiments, with four measurements taken on each surface and averaged to obtain the corresponding Ra IN and Ra OUT values. The experimental results were compared with the corresponding model predictions, as summarized in Table **7**.

The experimental results showed good agreement with the model predictions for all three optimization solutions. For the multi-response optimization, the measured values were 13.602 μm for Ra OUT and 13.779 μm for Ra IN, compared with predicted values of 13.228 μm and 13.648 μm, respectively. The corresponding relative deviations were −2.83% and −0.96%. For the individual optimization of Ra OUT, the measured external roughness was 12.802 μm, compared with a predicted value of 13.216 μm, resulting in a relative deviation of 3.13%. The corresponding internal roughness was 13.426 μm, compared with a predicted value of 13.702 μm, with a relative deviation of 2.01%. Similarly, for the individual optimization of Ra IN, the measured internal roughness was 13.304 μm, compared with a predicted value of 13.455 μm, corresponding to a relative deviation of 1.12%. The external roughness measured for this specimen was 13.662 μm, compared with a predicted value of 13.384 μm, resulting in a relative deviation of −2.08%.

Table 7: Experimental Confirmation Results for the Optimized Settings

					Experimental		Predicted		Relative deviation	
Run	**Target**	**Flow (%)**	**Layer (mm)**	**Speed (mm/s)**	**Ra OUT (μm)**	**Ra IN (μm)**	**Ra OUT (μm)**	**Ra IN (μm)**	**Ra OUT (%)**	**Ra IN (%)**
1	**Ra OUT & Ra IN**	90.9	0.2	116	13.602	13.779	13.228	13.648	-2.83%	-0.96%
2	**Ra OUT**	92.7	0.2	120	12.802	13.426	13.216	13.702	3.13%	2.01%
3	**Ra IN**	89.7	0.2	84.4	13.662	13.304	13.384	13.455	-2.08%	1.12%

Overall, all six comparisons between the experimental and predicted roughness values showed relative deviations below 3.2%. These results provide experimental confirmation of the optimization solutions and indicate good agreement between the measured responses and the predictions of the developed quadratic regression models at the selected processing conditions. These findings demonstrate the agreement between the experimental results and model predictions for the selected optimized processing conditions, providing further support for the applicability of the developed regression models within the investigated parameter range.

4. CONCLUSIONS

This study investigated the effects of flow rate, layer height, and printing speed on the internal and external surface roughness of FFF-manufactured Wood/PLA hollow cylindrical specimens. Based on the experimental measurements, regression modelling, statistical analysis, and multi-response optimization, the following conclusions can be drawn.

1. Layer height was the dominant process parameter associated with surface roughness. Increasing the layer height from 0.20 to 0.40 mm was accompanied by a substantial increase in both internal and external roughness. The measured values ranged from 13.650 to 29.716μm for the internal surface and from 13.163 to 26.875μm for the external surface. This behaviour is consistent with the geometric influence of layer deposition on the resulting surface profile.

2. The internal and external surfaces exhibited different responses to the investigated processing conditions. The minimum measured internal roughness was obtained at a flow rate of 80%, a layer height of 0.20mm, and a printing speed of 40mm/s, whereas the minimum measured external roughness occurred at a flow rate of 80%, a layer height of 0.20mm, and a printing speed of 80mm/s. These findings highlight the importance of considering both surface locations when evaluating the surface quality of hollow cylindrical components.

3. The quadratic regression models provided a very good fit to the experimental data, with coefficients of determination of 99.60% for internal roughness and 99.58% for external roughness. However, the absence of independent replicate specimens limits the assessment of experimental repeatability. Further experiments under independent conditions are required to evaluate the generalizability and robustness of the models.

4. Multi-response optimization identified a model-predicted candidate combination (Flow: 90.9%, Layer: 0.20mm, Speed: 116.0mm/s) achieving a composite desirability of 0.998. Confirmatory experimental testing at the optimized conditions demonstrated excellent agreement with model predictions, yielding relative deviations below 3.2% and verifying the reliability of the optimization approach.

Overall, the findings highlight the dominant influence of layer height and the importance of evaluating internal and external surface roughness separately. Future work should include independent replicate specimens across the full design space and evaluation under additional dynamic or environmental conditions. Further investigation of the mechanical and environmental performance of Wood/PLA components would also be necessary to establish their suitability and potential benefits for specific applications.

CONFLICT OF INTEREST

The authors declared no conflicts of interest.

AUTHORS' CONTRIBUTION

Conceptualization, E.S., N.E. and P.K.; Methodology, E.S., A.M., N.E., V.P. and P.K.; Validation, E.S., A.M., N.E., V.P., N.V. and P.K.;

Formal analysis, E.S., N.E., V.P., N.V. and P.K.; Investigation, E.S., A.M., N.E., V.P. and P.K.; Resources, E.S., N.V. and P.K.; Data curation, E.S., A.M., N.E. and P.K.; Writing – original draft, E.S., N.E. and P.K.; Writing – review & editing, E.S., A.M., N.E., V.P., N.V. and P.K.; Visualization, E.S., A.M., V.P., N.V. and P.K.; Supervision, E.S., N.E. and P.K.

All authors have read and agreed to the published version of the manuscript.

ACKNOWLEDGEMENTS

The authors would like to express their sincere gratitude to the University of Western Macedonia for funding the publication fees of the present paper.

REFERENCES

[1] Ranjan R, Kumar D, Kundu M, Chandra Moi S. A critical review on Classification of materials used in 3D printing process. Materials Today: Proceedings. 2022; 61: 43-9. https://doi.org/10.1016/j.matpr.2022.03.308

[2] Bhargava SK, Ramakrishna S, Brandt M, Selvakannan Pr, editors. Additive Manufacturing for Chemical Sciences and Engineering [Internet]. Singapore: Springer Nature Singapore; 2022 [cited 2026 Oct 9]. Available from: https://link.springer.com/10.1007/978-981-19-2293-0. https://doi.org/10.1007/978-981-19-2293-0

[3] Shahrubudin N, Lee TC, Ramlan R. An Overview on 3D Printing Technology: Technological, Materials, and Applications. Procedia Manufacturing. 2019; 35: 1286-96. https://doi.org/10.1016/j.promfg.2019.06.089

[4] Li X, Lin Y, Liu M, Meng L, Li C. A review of research and application of polylactic acid composites. J of Applied Polymer Sci. 2023 Feb 15; 140(7): e53477. https://doi.org/10.1002/app.53477

[5] Wang X, Zhao L, Fuh JYH, Lee HP. Effect of Porosity on Mechanical Properties of 3D Printed Polymers: Experiments and Micromechanical Modeling Based on X-ray Computed Tomography Analysis. Polymers. 2019 Jul 5; 11(7): 1154. https://doi.org/10.3390/polym11071154

[6] Kartal F, Kaptan A. Beyond Datasheets: A Comparative Evaluation of Standard and Technical Filaments in High-Speed FDM 3D Printing. KUJES. 2025 Jun 25; 11(1): 1-11. https://doi.org/10.55385/kastamonujes.1603181

[7] Bhayana M, Singh J, Sharma A, Gupta M. A review on optimized FDM 3D printed Wood/PLA bio composite material characteristics. Materials Today: Proceedings. 2023 Mar; S2214785323010714. https://doi.org/10.1016/j.matpr.2023.03.029

[8] Buj-Corral I, Bagheri A, Sivatte-Adroer M. Effect of Printing Parameters on Dimensional Error, Surface Roughness and Porosity of FFF Printed Parts with Grid Structure. Polymers. 2021 Apr 9; 13(8): 1213. https://doi.org/10.3390/polym13081213

[9] Pratama J, Mayanda N, Sugiyanto D. Effect of Extruder Temperature on Dimensional Accuracy and Surface Roughness of Fused Deposition Modeled (FDMed) PLA and PLA/Wood Composite. Vol. 24. 2022; 24(2).

[10] Fountas NA, Zaoutsos S, Chaidas D, Kechagias JD, Vaxevanidis NM. Statistical modelling and optimization of mechanical properties for PLA and PLA/Wood FDM materials. Materials Today: Proceedings. 2023; 93: 824-30. https://doi.org/10.1016/j.matpr.2023.08.276

[11] Joseph Arockiam A, Karthikeyan Subramanian, Padmanabhan RG, Rajeshkumar Selvaraj, Dilip Kumar Bagal, Rajesh S. A review on PLA with different fillers used as a filament in 3D printing. Materials Today: Proceedings. 2022; 50: 2057-64. https://doi.org/10.1016/j.matpr.2021.09.413

[12] Al-Zaidi AAMA, Al-Gawhari FJJ. Types of Polymers Using in 3D Printing and Their Applications: A Brief Review. ejtas. 2023 Nov 1; 1(6): 978-85. https://doi.org/10.59324/ejtas.2023.1(6).94

[13] Kyratsis V, Tzotzis A, Korlos A, Efkolidis N. Investigation of the Fabrication Parameters' Influence on the Tensile Strength of 3D-Printed Copper-Filled Metal Composite Using Design of Experiments. JMMP. 2024 Dec 2; 8(6): 278. https://doi.org/10.3390/jmmp8060278

[14] Minaoglou P, Tzotzis A, Efkolidis N, Kyratsis P. Influence of the 3D Printing Fabrication Parameters on the Tensile Properties of Carbon-Based Composite Filament. Applied Mechanics. 2024 Oct 24; 5(4): 745-61. https://doi.org/10.3390/applmech5040041

[15] Kechagias JD, Zaoutsos SP. An assessment of PLA/wood with PLA core sandwich multilayer component tensile strength under different 3D printing conditions. Journal of Manufacturing Processes. 2024 Dec; 131: 1240-9. https://doi.org/10.1016/j.jmapro.2024.09.098

[16] Krapež Tomec D, Schöflinger M, Leßlhumer J, Žigon J, Humar M, Kariž M. Effect of thermal modification of wood on the rheology, mechanical properties and dimensional stability of wood composite filaments and 3D-printed parts. Wood Material Science & Engineering. 2024 Nov; 19(6): 1251-65. https://doi.org/10.1080/17480272.2024.2316740

[17] Bambu Lab. Safety Data Sheet (SDS): Bambu PLA Wood [Internet]. Bambu Lab; 2025 Jul [cited 2026 Oct 27]. Report SDS20250723A16. Available from: https://store.bblcdn.com/s7/default/d6c961ed06964581815e31ec1816e254/SDS20250723SA16_Bambu_PLA_Wood.pdf

[18] Bambu Lab. PLA Wood Technical Data Sheet [Internet]. Bambu Lab; [cited 2026 Oct 27]. Available from: https://store.bblcdn.com/s4/default/6fda0ae88e5a4e66bb5d58f2968eee42/Bambus_PLA_Wood_Technical_Data_Sheet.pdf

[19] Reverte JM, Caminero MÁ, Chacón JM, García-Plaza E, Núñez PJ, Becar JP. Mechanical and Geometric Performance of PLA-Based Polymer Composites Processed by the Fused Filament Fabrication Additive Manufacturing Technique. Materials. 2020 Apr 19; 13(8): 1924. https://doi.org/10.3390/ma13081924

[20] Suvanjumrat C, Chansoda K, Chookaew W. Additive manufacturing advancement through large-scale screw-extrusion 3D printing for precision parawood powder/PLA furniture production. Cleaner Engineering and Technology. 2024 Jun; 20: 100753. https://doi.org/10.1016/j.clet.2024.100753

[21] Tahir M, Seyam AF. Greening Fused Deposition Modeling: A Critical Review of Plant Fiber-Reinforced PLA-Based 3D-Printed Biocomposites. Fibers. 2025 May 14; 13(5): 64. https://doi.org/10.3390/fib13050064

https://doi.org/10.12974/2311-8717.2026.14.15

© 2026 Semertzidou *et al.*
This is an open-access article licensed under the terms of the Creative Commons Attribution License (http://creativecommons.org/licenses/by/4.0/), which permits unrestricted use, distribution, and reproduction in any medium, provided the work is properly cited.